Spin excitations of the block-antiferromagnetic state in K_{0.8}Fe_{1.6}Se_{2}

Yi-Zhuang You, Hong Yao, and Dung-Hai Lee

Spin excitations of the block-antiferromagnetic state in $K_{0.8}Fe_{1.6}Se_2$

Yi-Zhuang You[1,3], Hong Yao[1,2], Dung-Hai Lee[1,2]

[1] *Department of Physics, University of California at Berkeley, Berkeley, CA 94720, USA,*
[2] *Materials Sciences Division, Lawrence Berkeley National Laboratory, Berkeley, CA 94720, USA*
[3] *Institute for Advanced Study, Tsinghua University, Beijing, 100084, China*
(Dated: April 22, 2011)

We study the spin excitations of the newly discovered block-antiferromagnetic state in $K_{0.8}Fe_{1.6}Se_2$. Due to the nature of block antiferromagnetism, we expect spin wave excitations to possess both Goldstone modes and optical branches. We use a simple model Hamiltonian to demonstrate this idea, and compute the dispersion and the dynamic spin structure factor using explicit parameters. Our prediction can be directly tested by inelastic neutron scattering experiments.

PACS numbers:

The discovery of the $K_xFe_{2-y}Se_2$[1] system stirred up a new wave of excitement in the field of iron-based superconductors. $K_xFe_{2-y}Se_2$ are isostructural to the "122"-family of iron pnictides, e.g. $BaFe_2As_2$. At ambient pressure they exhibit the highest superconducting transition temperature $\approx 33K$ among iron chalcogenides[1].

Very recently a neutron scattering experiment[2] showed that at the special composition $x = 0.8, y = 0.4$ $K_{0.8}Fe_{1.6}Se_2$ exhibits a novel structure and magnetic state. In particular for $T < 578K$ the Fe vacancies (which cause the deficiency of the iron content from 2 Fe per formula unit) form a $\sqrt{5} \times \sqrt{5}$ superstructure in each Fe plane as shown in Fig. 1(a). The nearest Fe-Fe distance between the four irons in each $\sqrt{5} \times \sqrt{5}$ unit cell is slightly smaller than that between the neighboring cells[2, 5]. Moreover for $T < 559K$ the system becomes magnetic. The magnetic moments of the four irons in each $\sqrt{5} \times \sqrt{5}$ unit cell align ferromagnetically along the crystalline c-axis. These aligned "super-moments" stagger from cell to cell to form a block-checkerboard antiferromagnetic pattern[2]. At low temperatures the ordered moment per iron is approximately equal to $3.3\mu_B$. Since the iron valence is found to be $+2$[4], and LDA calculations find $K_{0.8}Fe_{1.6}Se_2$ to be an insulator with an approximate 0.6eV energy gap[3, 5], this implies that each iron is in spin 2 state.

It is well known that lattice distortion and iron distribution can affect the nature of the magnetic order[6]. For example, in most of the iron pnictide materials a tetragonal to orthorhombic lattice distortion accompanies the colinear antiferromagnetic order; where the iron moments align in one direction but stagger in the other. For FeTe the so-called bi-colinear antiferromagnetic order is accompanied by a monoclinic lattice distortion. In addition, excess Fe's are known to modify the magnetic order from commensurate to incommensurate order. We view $K_{0.8}Fe_{1.6}Se_2$ as a special and more dramatic example where a periodic modulation of the Fe distribution and the resultant lattice distortion stabilize an even more exotic magnetic order.

In addition to the novel structural and magnetic or-

dering, transport measurement has shown samples with composition close to $K_{0.8}Fe_{1.6}Se_2$ are superconductors with transition temperature in the neighborhood of 30K. Ref.[2, 4] advocates the microscopic coexistence of superconductivity and block-antiferromagnetism. Others raises doubt about this conclusion[7]. We will restrain from discussing superconductivity in this paper before the experimental situation is clear. In the following we shall focus on the magnetic property of $K_{0.8}Fe_{1.6}Se_2$.

Given the novel magnetic order described above it is interesting to ask what is the nature of the spin excitations. In particular the block-antiferromagnetic order suggests in addition to the usual gapless Goldstone modes (which can exhibit a small gap in the presence of spin-orbit interaction), there should be "optical" spin wave branches analogous to the optical phonons in crystals with more than one atom per unit cell. Given the fact that the ordering moment is relatively large, the linearized Holstein-Primikov Hamiltonian should be a very good approximate description of the low energy spin dynamics.

In Ref.[3] an effective spin Hamiltonian has been used to fit the LDA results. The Hamiltonian involves intra-block nearest and second neighbor interactions J_1, J_2 and
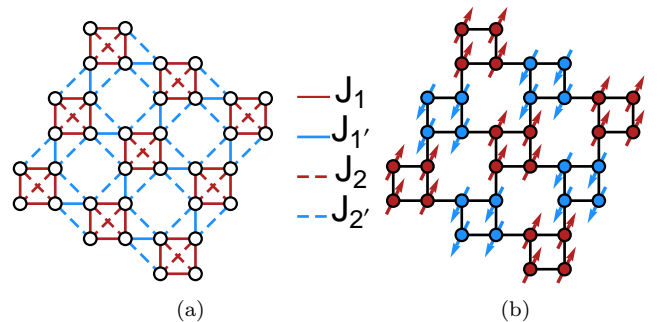

FIG. 1: (Color online) (a) The schematic representation of the vacancy ordered $\sqrt{5} \times \sqrt{5}$ lattice structure in each iron plane. Circles represent irons and the solid and dashed lines represent different types of spin interaction. (b) The ordered spin configuration according to Ref.[2]. The spins point along the c-axis (out of plane).

the inter-block nearest and second neighbor interactions $J_{1'}, J_{2'}$. Because the iron magnetic moments are observed to align along the c-axis (perpendicular to the iron planes)[2], there should presumably be a spin anisotropy term in the Hamiltonian. The minimum Hamiltonian we consider reads:

$$H = \frac{1}{2} \sum_{i,j} J_{ij} \boldsymbol{S}_i \cdot \boldsymbol{S}_j - \Delta \sum_i S_{iz}^2, \qquad (1)$$

where Δ is the spin anisotropy, and $J_{ij} = J_1 \Gamma_{ij}^1 + J_{1'} \Gamma_{ij}^{1'} + J_2 \Gamma_{ij}^2 + J_{2'} \Gamma_{ij}^{2'}$ with Γ_{ij}^b ($b = 1, 1', 2, 2'$) being the adjacency matrix defined by

$$\Gamma_{ij}^b = \begin{cases} 1 & : (i,j) \text{ form the shortest } b\text{-type bounds}, \\ 0 & : \text{otherwise.} \end{cases}$$
$$(2)$$

The bond types are illustrated in Fig. 1(a). The classical ground state has the block-AFM order as shown in Fig. 1(b). For later convenience, the sign factor $\zeta_i = \pm 1$ for $i \in$ the up(down)-spin block is defined here.

In the following we assume each spin has $S = 2$. To study the spin wave excitations we use the linearized Holstein-Primakoff (HP) transformations $S_i^z = \zeta_i(S - a_i^\dagger a_i)$ and $S_i^x = \sqrt{2S}(a_i^\dagger + a_i)/2$. Using the magnetic unit cell with 8 Fe atoms, the spin Hamiltonian can be written in terms of HP bosons in the momentum space as

$$H = \frac{1}{2} S \left[\sum_{\boldsymbol{q}} \phi_{\boldsymbol{q}\alpha}^\dagger J_{\alpha\beta}(\boldsymbol{q}) \phi_{\boldsymbol{q}\beta} + O(1/S) \right], \qquad (3)$$

where $\phi_{\boldsymbol{q}\alpha}^\dagger = (a_{\boldsymbol{q}\alpha}^\dagger, a_{-\boldsymbol{q}\alpha})$ and

$$\begin{aligned} J_{\alpha\beta}(\boldsymbol{q}) &= \left[J_1 \Gamma_{\alpha\beta}^1(\boldsymbol{q}) + J_2 \Gamma_{\alpha\beta}^2(\boldsymbol{q}) + J_0 \delta_{\alpha\beta} \right] \sigma_0 \\ &+ \left[J_{1'} \Gamma_{\alpha\beta}^{1'}(\boldsymbol{q}) + J_{2'} \Gamma_{\alpha\beta}^{2'}(\boldsymbol{q}) \right] \sigma_1. \end{aligned} \qquad (4)$$

Here α, β label the 8 sites in the unit cell, $J_0 = 2\Delta - 2J_1 + J_{1'} - J_2 + 2J_{2'}$, and σ_i denote the Pauli matrices (σ_0 being

the 2×2 identity matrix). The Fourier transform of the adjacency matrix reads

$$\Gamma_{\alpha\beta}^b(\boldsymbol{q}) = \sum_{j,(i\in\alpha; j\in\beta)} \Gamma_{i,j}^b e^{i\boldsymbol{q}\cdot(\boldsymbol{r}_i - \boldsymbol{r}_j)}. \qquad (5)$$

Here $\boldsymbol{r}_i$ denotes the position vector of site i, and $\boldsymbol{q} \in$ the magnetic Brillouin zone (MBZ). Use the the Fe-Fe bond directions as $\hat{x}$ and $\hat{y}$ and set nearest Fe-Fe bond length to unity, the MBZ is spanned by the reciprocal lattice vectors $\boldsymbol{Q}_1 = (3\pi/5, \pi/5)$ and $\boldsymbol{Q}_2 = (-\pi/5, 3\pi/5)$. The high symmetry points are defined as $\Gamma = (0,0)$, $X' = \boldsymbol{Q}_1/2$, $Y' = \boldsymbol{Q}_2/2$, $M' = (\boldsymbol{Q}_1 + \boldsymbol{Q}_2)/2$ as shown in Fig. 2(a).

For each $\boldsymbol{q}$ we perform the Bogoliubov transformation on the 16×16 matrix $SJ(\boldsymbol{q})$ to obtain the spin wave operators and dispersions. This can be achieved by solving the generalized eigenvalue problem

$$\sum_\beta SJ_{\alpha\beta}(\boldsymbol{q}) \begin{pmatrix} u_{n\boldsymbol{q}\beta} \\ v_{n\boldsymbol{q}\beta} \end{pmatrix} = \Omega_{n\boldsymbol{q}} \sigma_3 \begin{pmatrix} u_{n\boldsymbol{q}\alpha} \\ v_{n\boldsymbol{q}\alpha} \end{pmatrix}, \qquad (6)$$

where $\Omega_{n\boldsymbol{q}} \geq 0$ are the spin wave dispersions and $n = 1, \cdots, 8$ denotes the band index (keeping only the positive eigenvalue solutions). Note that σ_3 is needed in Eq.(6) for Bogoliubov transformation of bosons. The wave functions are normalized to $\sum_\alpha (|u_{n\boldsymbol{q}\alpha}|^2 - |v_{n\boldsymbol{q}\alpha}|^2) = 1$. The corresponding spin wave creation operator is given by $b_{n\boldsymbol{q}}^\dagger = \sum_\alpha u_{n\boldsymbol{q}\alpha} a_{\boldsymbol{q}\alpha}^\dagger + v_{n\boldsymbol{q}\alpha} a_{-\boldsymbol{q}\alpha}$. Due to the Goldstone theorem, we anticipate two branches of degenerate gapless spin wave modes (which would be slightly gapped by the spin anisotropy). However, since there are eight spins per magnetic unit cell, there must remain 6 gapful collective branches in the spin wave dispersion. These gapped spin wave modes are like optical phonons in the crystal with multi-atom per unit cell. These gapped spin waves are, in general, twofold degenerate.

To explicitly demonstrate the above anticipation in the absence of the uniaxial anisotropy ($\Delta = 0$) we adapt the parameters $J_1 = -4$meV, $J_{1'} = 1$meV, $J_2 = 3$meV, $J_{2'} = 12$meV. Aside from J_2 the above values are given in Ref.[3] by fitting to LDA calculations. The reason we slightly reduced J_2 is because using the value given in Ref.[3] we find the spin wave excitations are unstable. For the chosen parameters, the resulting spin-wave dispersion is shown as the black lines in Fig. 2(b). As expected, there are two degenerate Goldstone modes. The rest of the spin wave excitations form three doubly degenerate branches. In the following we shall refer to them as the "optical" spin waves. Although the details of the spin wave dispersion can depend on the specific parameter values, we emphasize that the qualitative conclusion, namely, the presence of both Goldstone mode and optical spin wave branches will not be affected. The presence of the optical spin wave is a direct consequence of the block antiferromagnetism.

To demonstrate the effect of the uniaxial anisotropy we set $\Delta = 0.08$meV and illustrate the corresponding
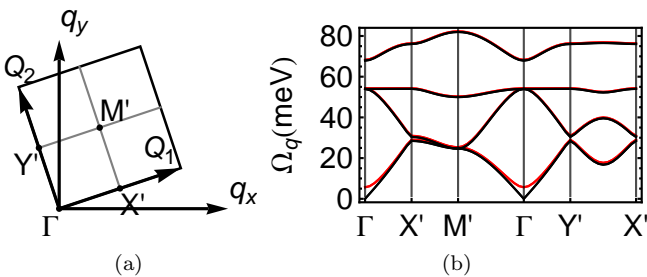

FIG. 2: (Color online) (a) The magnetic Brillouin zone. (b) The spin wave spectrum. The black lines represent the dispersion in the absence of the spin anisotropy. The red lines represent the dispersion in the presence of spin anisotropy. As expected, spin anisotropy gaps the Goldstone mode.

spin wave dispersion using the red lines in Fig. 2(b). The gap of the Goldstone mode at $\boldsymbol{q} = 0$ is found to be $2S\sqrt{\Delta(\Delta + J_{1'} + 2J_{2'})} \approx 6\text{meV}$. The optical modes are not much affected by the anisotropy as long as Δ is much smaller than the magnitude of all coupling constants.

In table I, we list the analytical expressions for the optical spin wave excitation energies at Γ and M' (for $\Delta = 0$). (Analytical expressions at other momentum points are not known to us.) In conjunction with the neutron data they can be used to determine the effective coupling constants $J_{1,2}$ and $J_{1',2'}$.

TABLE I: Table of spin wave excitation energies ($\Delta = 0$)

Momentum	Energy	Degeneracy
	0	2
Γ	$2S\sqrt{(J_1 + J_2 - J_{2'})(J_1 - J_{1'} + J_2 - J_{2'})}$	4
	$2\sqrt{2}S\sqrt{(2J_1 - J_{1'})(J_1 - J_{2'})}$	2
	$2S\sqrt{J_1^2 - (J_{1'} - 2J_2 + 2J_{2'})J_1 + J_2(J_2 - 2J_{2'}) + J_{1'}(J_{2'} - J_2)}$	4
M'	$2S\lvert J_1 + \sqrt{(J_1 - J_{2'})(J_1 - J_{1'} - J_{2'})}\rvert$	2
	$2S\lvert J_1 - \sqrt{(J_1 - J_{2'})(J_1 - J_{1'} - J_{2'})}\rvert$	2

Due to quantum and thermal fluctuations, the magnetization $\lvert\langle S_i^z\rangle\rvert$ is reduced from S to $\lvert\langle S_i^z\rangle\rvert = S - \delta S$, where the correction δS is given by

$$
\begin{aligned}
\delta S &= \int_{\boldsymbol{q}\in\text{MBZ}} \frac{d^2\boldsymbol{q}}{(2\pi/\sqrt{5})^2} \langle a_{\boldsymbol{q}\alpha}^\dagger a_{\boldsymbol{q}\alpha}\rangle, \\
&= \int_{\boldsymbol{q}\in\text{MBZ}} \frac{d^2\boldsymbol{q}}{(2\pi/\sqrt{5})^2} \sum_n \Big[\lvert u_{n\boldsymbol{q}\alpha}\rvert^2 n_B(\Omega_{n\boldsymbol{q}}) \quad (7) \\
&\qquad + \lvert v_{n\boldsymbol{q}\alpha}\rvert^2 (n_B(\Omega_{n\boldsymbol{q}}) + 1) \Big],
\end{aligned}
$$

where n_B is the Bose-Einstein distribution function and there is no summation over α. The moment correction δS is found to be the same on all sites. For the parameter $J_1 = -4, J_{1'} = 1, J_2 = 3, J_{2'} = 12, \Delta = 0.08\text{meV}$, we find $\delta S = 0.32$ at zero temperature. This amounts to a magnetic moment per iron equal to $2 \times (S - \delta S) = 3.36$ Bohr magneton (μ_B), in good agreement with the experimental deduced value. The temperature dependence of the ordering moment (per iron) is shown in Fig. 4(a).

To the same leading order approximation, the zero-temperature dynamic structure factor is given by

$$
S_\perp(\boldsymbol{q}, \omega) = \sum_n A_{n\boldsymbol{q}} \delta(\omega - \Omega_{n\boldsymbol{q}}), \quad (8)
$$

where the spectral weight $A_{n\boldsymbol{q}}$ reads

$$
A_{n\boldsymbol{q}} = \sum_{\alpha,\beta} (u_{n\boldsymbol{q}\alpha}^* + v_{n\boldsymbol{q}\alpha}^*)(u_{n\boldsymbol{q}\beta} + v_{n\boldsymbol{q}\beta}) e^{i\boldsymbol{q}\cdot(\boldsymbol{r}_\alpha - \boldsymbol{r}_\beta)}. \quad (9)
$$

Note that $A_{n\boldsymbol{q}}$ is not periodic with reciprocal magnetic unit vector $\boldsymbol{Q}_1$ and $\boldsymbol{Q}_2$ even though spin wave energy $\Omega_{n\boldsymbol{q}}$ is. This is similar to the matrix element effect in angle-resolved photoemission experiments. Fig. 3 shows the dynamic structure factor along the Γ-M' cut. In inelastic neutron scattering experiments, the Γ-point "optical" modes will be observable at $(2\pi/5, 4\pi/5)$ point, and the M'-point "optical" modes will be visible at $(\pi, 0)$ point.

It is also straightforward to compute the uniform susceptibility. The transverse uniform susceptibility reads

$$
\chi_\perp = \frac{S\mu_B^2}{128} \lim_{\boldsymbol{q}\to 0} \sum_{n,\alpha,\beta} \frac{(u_{n\boldsymbol{q}\alpha}^* + v_{n\boldsymbol{q}\alpha}^*)(u_{n\boldsymbol{q}\beta} + v_{n\boldsymbol{q}\beta})}{\Omega_{n\boldsymbol{q}}}, \quad (10)
$$

which is independent of temperature in the low temperature regime. Using our parameters, it can be evaluated to $\chi_\perp = 2.49\mu_B^2\text{eV}^{-1}$. The longitudinal uniform susceptibility is given by

$$
\chi_\parallel = \frac{\mu_B^2}{256} \sum_{n,\boldsymbol{q}} \left[\sum_\alpha \zeta_\alpha (\lvert u_{n\boldsymbol{q}\alpha}\rvert^2 + \lvert v_{n\boldsymbol{q}\alpha}\rvert^2) \right]^2 n_B'(\Omega_{n\boldsymbol{q}}), \quad (11)
$$

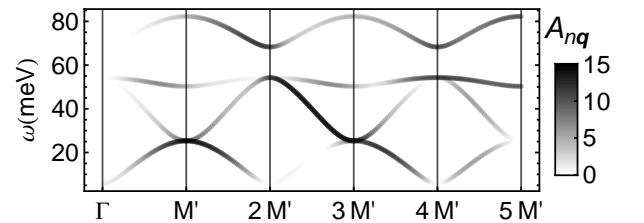
FIG. 3: Dynamic spectral function along the cut through the Γ-M' line. pM' denotes the momentum point of $(p\pi/5, 2p\pi/5)$. $2M'$ and $4M'$ are equivalent to Γ point in the MBZ, while $3M'$ and $5M'$ are equivalent to M'. The spin wave dispersion is plotted using the spectral weight of the dynamic spectral function as darkness.
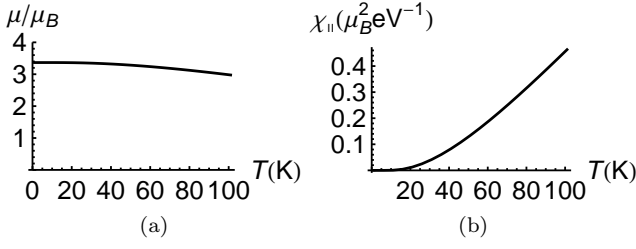
FIG. 4: Temperature dependence of (a) the per-iron magnetic moment, and (b) the longitudinal uniform susceptibility.

where where $\zeta_\alpha = \pm 1$ for α residing in spin up or down block respectively, and n'_B denotes the derivative of Bose-Einstein distribution function. Fig. 4(b) shows the temperature dependence of $\chi_\parallel$. Below the temperature scale of the spin gap (~ 50K), $\chi_\parallel$ exhibit exponential temperature dependence. While above that temperature scale, the linear-T behavior $\chi_\parallel \propto T$ can be observed.

In conclusion we have studied the spin wave excitations of the block-antiferromagnetic $K_{0.8}Fe_{1.6}Se_2$ using an effective spin model suggested by LDA calculation. There are both the Goldstone modes and the "optical" spin wave branches. After the spin wave correction, the ordering moment is found to be $\approx 3.4\mu_B$ per iron at low temperatures, which is close to the observed value. The observation of the optical spin wave modes will constitute a spectacular supporting evidence for the block antiferromagnetism.

Currently we do not have a good understanding of the block-antiferromagnetism and its relation to the structural distortion from microscopic point of view. Understanding it can shed light on the local electronic structure and correlation for the newly discovered $K_xFe_{2-y}Se_2$ and other pnictides.

[1] Jiangang Guo, Shifeng Jin, Gang Wang, Shunchong Wang, Kaixing Zhu, Tingting Zhou, Meng He, and Xiaolong Chen, Phys. Rev. B **82**, 180520(R) (2010).

[2] Wei Bao, Q. Huang, G. F. Chen, M. A. Green, D. M. Wang, J. B. He, X. Q. Wang, Y. Qiu, arXiv:1102.0830.

[3] C. Cao and J. Dai, arXiv:1102.1344.

[4] Wei Bao, G. N. Li, Q. Huang, G. F. Chen, J. B. He, M. A. Green, Y. Qiu, D. M. Wang, J. L. Luo, arXiv:1102.3674.

[5] X.-W. Yan, M. Gao, Z.-Y. Lu, and T. Xiang, arXiv:1102.2215.

[6] For a review of the magnetic order in other iron-based materials, see J. Lynn and P. Dai, Physica C, 469, 469-476 (2009).

[7] Fei Han, Bing Shen, Zhen-Yu Wang, Hai-Hu Wen, arXiv:1103.1347.